Doxorubicin causes lesions in the electron transport system of skeletal muscle mitochondria that are associated with a loss of contractile function

Received for publication, March 13, 2019, and in revised form, October 25, 2019 Published, Papers in Press, November 5, 2019, DOI 10.1074/jbc.RA119.008426

Michael D. Tarpey[‡], Adam J. Amorese[‡], Nicholas P. Balestrieri[‡], Kelsey H. Fisher-Wellman[‡§], and Espen E. Spangenburg[‡§1]

From the [‡]Department of Physiology and the [§]East Carolina Diabetes and Obesity Institute, Brody School of Medicine, East Carolina University, Greenville, North Carolina 27834

Edited by Qi-Qun Tang

Doxorubicin is an anthracycline-based chemotherapeutic that causes myotoxicity with symptoms persisting beyond treatment. Patients experience muscle pain, weakness, fatigue, and atrophy, but the underlying mechanisms are poorly understood. Studies investigating doxorubicin-induced myotoxicity have reported disrupted mitochondrial function. Mitochondria are responsible for regulating both cellular energy status and Ca^{2+} handling, both of which impact contractile function. Moreover, loss of mitochondrial integrity may initiate muscle atrophy. Skeletal muscle mitochondrial dysregulation may therefore contribute to an overall loss of skeletal muscle quality and performance that may be mitigated by appropriately targeted mitochondrial therapies. We therefore assessed the impact of doxorubicin on muscle performance and applied a multiplexed assay platform to diagnose alterations in mitochondrial respiratory control. Mice received a clinically relevant dose of doxorubicin delivered systemically and were euthanized 72 h later. We measured extensor digitorum longus and soleus muscle forces, fatigue, and contractile kinetics *in vitro*, along with Ca^{2+} uptake in isolated sarcoplasmic reticulum. Isolated skeletal muscle mitochondria were used for real-time respirometry or frozen for protein content and activity assays. Doxorubicin impaired muscle performance, which was indicated by reduced force production, fatigue resistance, and sarcoplasmic reticulum–Ca^{2+} uptake, which were associated with a substrate-independent reduction in respiration and membrane potential but no changes in the NAD(P)H/$NAD(P)^+$ redox state. Protein content and dehydrogenase activity results corroborated these findings, indicating that doxorubicin-induced mitochondrial impairments are located upstream of ATP synthase within the electron transport system. Collectively, doxorubicin-induced lesions likely span mitochondrial complexes I–IV, providing potential targets for alleviating doxorubicin myotoxicity.

Doxorubicin is member of the anthracycline drug class commonly used to treat a range of cancers and has attracted considerable attention because of its cardiotoxic side effects. Doxorubicin and its metabolite, doxorubicinol, also accumulate in skeletal muscle (1, 2), resulting in a myotoxicity, which can persist long beyond the cessation of treatment (3). Patients treated with doxorubicin frequently experience muscle atrophy (4, 5), as well as symptoms of muscle weakness and fatigue (6, 7). Reduced force production and fatigue resistance may be a by-product of muscle degradation; however, performance declines have been reported in the absence of changes in muscle mass (8) and when accounting for muscle cross-sectional area (CSA)[2] (9), and thus muscle atrophy does not entirely account for the decline in muscle quality. Studies investigating doxorubicin myotoxicity are limited and contain considerable variability in experimental design, such as treatment dose and time course. In addition, some studies have assessed the effects of doxorubicin on contractile function via acute *in vitro* exposures (9–11), as opposed to systemic exposure, which more accurately reflects clinical practice. Meanwhile, studies using systemic exposure designs have produced contradictory results in the extensor digitorum longus and soleus (8, 12, 13) and in some instances have not accounted for muscle CSA (8, 12). Together, these variations limit the ability to discern the mechanism of doxorubicin-induced contractile disruption and to what extent these effects are fiber type–specific.

The concomitant emergence of dysregulated mitochondria following doxorubicin exposure (3, 13, 14) may explain the

This work was supported by National Institutes of Health Grant R01AR06660 (to E. E. S.). The authors declare that they have no conflicts of interest with the contents of this article. The content is solely the responsibility of the authors and does not necessarily represent the official views of the National Institutes of Health.

[1] To whom correspondence should be addressed. Present address: East Carolina Diabetes and Obesity Institute, Dept. of Physiology, Brody School of Medicine, 115 Heart Dr., East Carolina University, Greenville, NC 27834. Tel.: 252-737-5035; E-mail: spangenburge14@ecu.edu.

[2] The abbreviations used are: CSA, cross-sectional area; αKGDH, α-ketoglutarate dehydrogenase complex; ΔG_{ATP}, Gibbs free energy of ATP hydrolysis; $\Delta\Psi_m$, membrane potential; BCA, bicinchoninic acid assay; BCKDH, branched-chain keto-acid dehydrogenase complex; C*n*, complex *n* (where *n* is a Roman numeral); Doxo, doxorubicin-treated group; EDL, extensor digitorum longus; ETS, electron transport system; FCCP, carbonyl cyanide-4-phenylhydrazone; GDH, glutamate dehydrogenase; G/M, glutamate/malate; GOT2, aspartate aminotransferase; HADHA, hydroxyacyl CoA; IDH2, $NADP^+$-linked isocitrate dehydrogenase; IDH3, NAD-linked isocitrate dehydrogenase; JO_2, oxygen consumption; MDH2, malate dehydrogenase (mitochondrial); ME, malic enzyme; Pc/M, palmitoylcarnitine/malate; PCr, phosphate creatine; PDH, pyruvate dehydrogenase complex; PDK, pyruvate dehydrogenase kinase; P/M, pyruvate/malate; ROS, reactive oxygen species; R/S, rotenone/succinate; SERCA, sarco/endoplasmic reticulum Ca^{2+}-ATPase; SR, sarcoplasmic reticulum; TA, tibialis anterior; N, newton; CK, creatine kinase; PMFB, permeabilized muscle fiber bundle.

reduction in skeletal muscle performance, which depends upon mitochondrial regulation of cellular energy status and Ca^{2+} handling (15–17). Additionally, doxorubicin-exposed mitochondria up-regulate apoptosis (18, 19), leading to an elevation in skeletal muscle proteolysis (19), which may result in atrophy. Loss of mitochondrial quality may therefore be central to understanding doxorubicin-induced myotoxicity. Several studies have reported reduced skeletal muscle mitochondrial respiration and membrane potential (3, 13, 14), as well as time- and dose-dependent increases (3, 13, 14) or decreases (14) in reactive oxygen species (ROS) emission. However, only a limited number of studies have been reported in skeletal muscle mitochondria and were conducted under maximal ADP-stimulated conditions, which do not accurately reflect physiological thermodynamics and thus confound the findings. Additionally, mitochondrial respiratory function is a complex multifaceted process that incorporates mitochondrial dehydrogenases/enzymes, oxygen consumption (JO_2), membrane potential, redox status, and ATP production, but studies have traditionally focused on only one or two of these elements limiting their diagnostic potential (3, 13, 14). Meanwhile, attempts to identify the source of doxorubicin-induced mitochondriopathy have focused on oxidative damage. Although acute treatment with the reducing agent DTT has been shown to attenuate H_2O_2 emissions, respiratory defects were not mitigated (14). Thus, the relationship between doxorubicin and loss of skeletal muscle mitochondrial quality remains to be fully understood.

The present study was designed to determine the functional impact of acute systemic doxorubicin exposure on skeletal muscle. Measures were conducted 72 h post-treatment to study the initial phase of dysfunction, prior to extensive muscle wasting and oxidative damage to proteins and DNA. Fiber type–specific effects were assessed using the predominantly type IIx and IIb, and type I and IIa myofiber containing extensor digitorum longus (EDL) and soleus muscles, respectively. In addition, we employed a novel protocol for the assessment of isolated sarcoplasmic reticulum Ca^{2+} uptake across a physiologically relevant span of free energies of ATP hydrolysis. The study also applied a multiplexed diagnostic assay platform to assess doxorubicin-induced mitochondrial dysfunction under physiological energetic states, which has not previously been explored. Doxorubicin impaired force production regardless of fiber type, but specific force and half-relaxation defects were unique to the soleus, whereas a decline in fatigue resistance was notable in the EDL. Mitochondria exhibited notable declines in oxygen consumption and membrane potential; together, these are indicative of declining respiratory efficiency. In addition, we found no change to minor hyper-reductions in NAD(P)H/$NAD(P)^+$ redox status, as well as similar protein content and dehydrogenase enzyme activities between groups. Together, the present data indicated that doxorubicin-induced mitochondrial damage was largely confined to the electron transport system and was located upstream of ATP synthase, likely spanning complexes I–IV.

Results

Doxorubicin reduced body mass but was not associated with EDL or soleus muscle atrophy

Mice were administered equal volumes of PBS ($n = 8$) or doxorubicin (Doxo; $n = 9$) at a dose of 20 mg/kg body mass and euthanized 72 h postinjection. Consistent with previous reports, Doxo exposure decreased total body mass compared with PBS-treated controls (Fig. 1*A*; $-15.6 \pm 1.2\%$). Reductions in body mass were associated with relatively small changes in absolute EDL and soleus muscle mass, resulting in increases in relative muscle mass (Fig. 1*B*). However, the individual fiber CSA of the EDL and soleus were unaffected by Doxo treatment (Fig. 1, *C* and *D*), indicating that decreases in muscle mass did not contribute to Doxo-induced loss of body mass. Muscle fiber type of the EDL and soleus were unaffected by Doxo treatment, indicating that a shift in myofiber type was not responsible for any measured functional decline (Fig. 1*E*).

Doxorubicin caused skeletal muscle contractile dysfunction

To determine the impact of Doxo on contractile function, *in vitro* force production and fatigue protocols were performed using EDL and soleus muscles from PBS- and Doxo-treated mice. Absolute force (mN) production from both EDL and soleus muscles was reduced following Doxo treatment (Fig. 2*A*). This was accompanied by reductions in specific force (*i.e.* absolute force normalized to physiological CSA) in Doxo-exposed EDL and soleus muscles (Fig. 2*B*). Muscle fatigue (percent drop in initial force produced) was reduced by Doxo in EDL but unchanged in soleus muscles (Fig. 2*C*). Analysis of contractile kinetics revealed that reduced force production in the soleus was associated with a greater half-relaxation time but not in the EDL (Fig. 2*D*). Collectively, these findings suggest that impairments in contractile function are fiber type–specific and are not dependent on muscle atrophy, following acute systemic Doxo exposure.

Doxorubicin reduces the rate of sarcoplasmic reticulum Ca^{2+} uptake but does not alter muscle iron content

To address doxorubicin-induced contractile dysfunction, sarcoplasmic reticulum (SR) Ca^{2+} uptake rates were measured across a physiologic range of ATP free energies of hydrolysis (ΔG_{ATP}) using a creatine kinase (CK) clamp and additions of creatine phosphate (PCr). Importantly, the rate of Ca^{2+} uptake was greater in the presence of ΔG_{ATP} _14.70 *versus* −12.94 kcal/mol, demonstrating that SERCA-dependent Ca^{2+} uptake retains responsiveness to ATP free energy *in vitro* (Fig. 3*A*). Within group Ca^{2+} uptake rates also demonstrated significant sensitivity to ΔG_{ATP} −14.70 *versus* −12.94 kcal/mol (Fig. 3, *B* and *C*). With respect to Doxo exposure, Ca^{2+} uptake was depressed in SR isolated from Doxo-treated mice across all energetic states (Fig. 3*D*). Finally, measures of Fe^{2+}, Fe^{3+}, and total iron ($Fe^{2+} + Fe^{3+}$) were similar in gastrocnemius muscles between groups (Fig. 3*E*).

Doxorubicin alters bioenergetic efficiency in skeletal muscle mitochondria by impairing respiratory complex function

A mitochondrial diagnostics platform was leveraged to unbiasedly assess the impact of Doxo on skeletal muscle bioener-

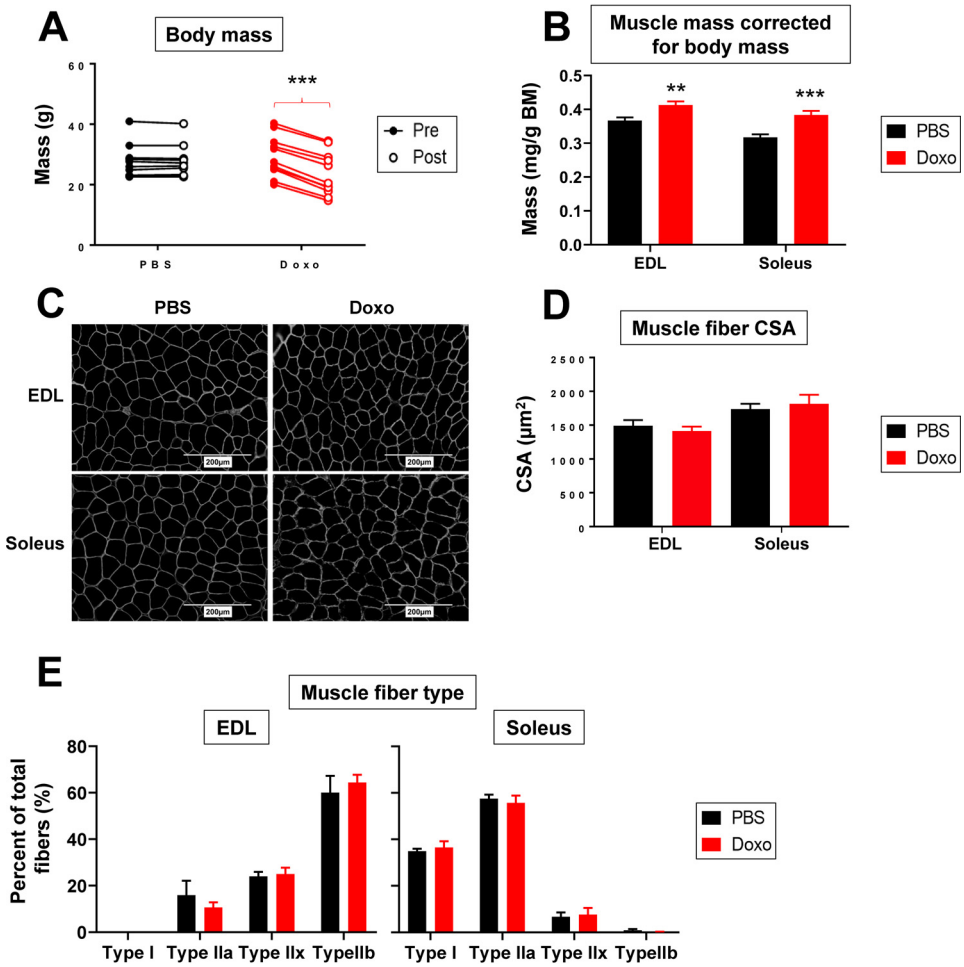

Figure 1. Doxorubicin causes loss of body mass but does not significantly reduce muscle mass and fiber CSA of EDL and soleus muscles. *A*, changes in body mass following treatment with PBS ($n = 10$) or Doxo ($n = 11$). *B*, muscle masses of the EDL and soleus corrected for body mass (PBS, $n = 8$; Doxo, $n = 9$). *C*, representative images of EDL and soleus muscle cross-sections. *D*, EDL and soleus muscle fiber CSA (PBS, $n = 4$; Doxo, $n = 4$). *E*, muscle fiber type composition of EDL and soleus muscle (PBS, $n = 4$; Doxo, $n = 4$). **, $p < 0.01$; ***, $p < 0.001$. The data are means ± S.E.

getic fluxes. To perform the assays, mitochondria were isolated from skeletal muscle of PBS- and Doxo-treated mice, and respiratory control was assessed across the same thermodynamic conditions as those used to measure SR–Ca^{2+} uptake. All assays were done using multiple substrate conditions (P/M, G/M, Pc/M, and R/S), each of which activates a unique set of matrix dehydrogenases and respiratory complexes.

Exposure to Doxo lowered mitochondrial JO_2, independent of ΔG_{ATP} or substrate condition (Fig. 4*A*). Although not conclusive using respirometry alone, the identical JO_2 effects induced by Doxo across multiple substrate conditions argues against bioenergetic lesions being localized to the matrix dehydrogenase network. With the exception of Pc/M, maximal uncoupled JO_2, assessed via the addition of FCCP at the end of the ΔG_{ATP} titration, remained lower in Doxo exposed mitochondria (Fig. 4*B*), suggesting that Doxo-mediated respiratory impairments are not caused by lesions in the phosphorylation system (*e.g.* ATP synthesis, ADP/ATP transport). Interestingly, although absolute respiratory sensitivity (*i.e.* the linear change in JO_2 for a given ΔG_{ATP} shift) was generally depressed by Doxo (Fig. 4*C*), normalization to the starting JO_2 eliminated respiratory sensitivity differences for all substrates but R/S (Fig. 4*D*). Collective analysis of all respirometry data suggests that doxorubicin impairs skeletal muscle bioenergetics via impinging on the respiratory complexes.

Parallel measurements of membrane potential ($\Delta\Psi_m$) and NAD(P)H/NAD(P)$^+$ redox state were performed to localize Doxo-mediated differences in respiratory control into one of three energy transduction control nodes: 1) ATP synthesis, 2) electron transport system (ETS), and 3) matrix dehydrogenases. Across all substrate conditions, $\Delta\Psi_m$ was decreased in Doxo-exposed mitochondria at each ΔG_{ATP} (Fig. 4*E*), as well as following normalization to JO_2 (Fig. 4*F*). In contrast, NAD(P)H/NAD(P)$^+$ redox was largely unaffected by Doxo exposure, except for hyper-reduction in the presence of R/S at the lowest ATP free energy (Fig. 4, *G* and *H*). Taken together, these data corroborate the respirometry data and suggest that bioenergetic impairments induced by doxorubicin are caused by ETS alterations.

Citrate synthase activity and mitochondrial dehydrogenases are minimally impacted by doxorubicin

Citrate synthase and ATP synthase (CV) activities were unaffected by Doxo exposure, suggesting mitochondrial content (20) per mitochondrial isolation was similar between PBS and Doxo groups (Fig. 5*A*). With one exception (pyruvate dehydro-

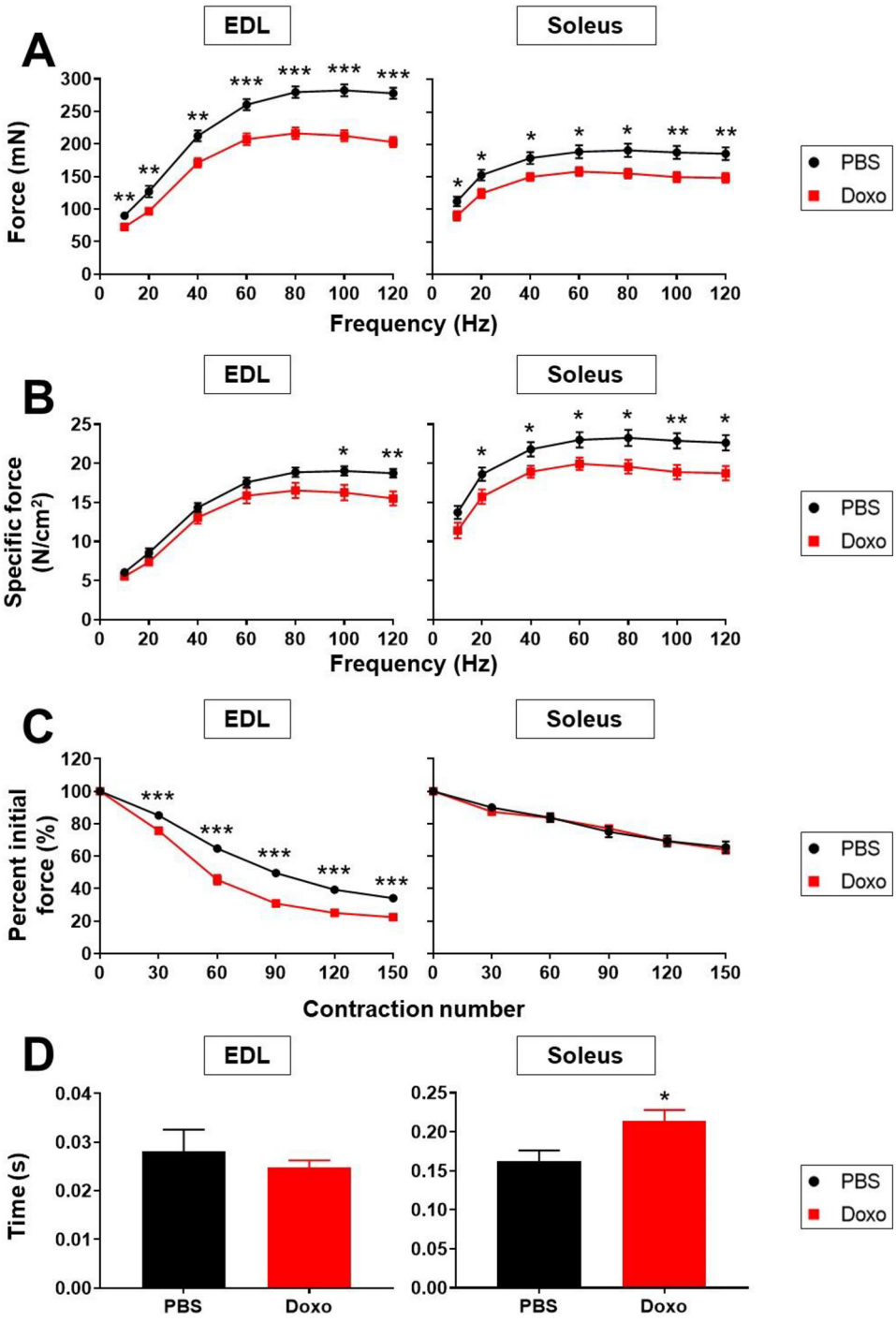

Figure 2. Doxorubicin causes skeletal muscle contractile dysfunction. *A*, force–frequency curve of absolute force (mN) production by EDL and soleus muscles. *B*, force–frequency curve of specific force (N/cm^2) production by EDL and soleus muscles. *C*, muscle fatigue (% change) in the EDL and soleus. *D*, half-relaxation time (seconds) of EDL and soleus muscles undergoing a 10-Hz stimulation. For all measures: PBS, $n = 8$; and Doxo, $n = 9$. *, $p < 0.05$; **, $p < 0.01$; ***, $p < 0.001$. The data are means ± S.E.

genase kinase (PDH)), no differences were observed across groups for various NAD(P)-linked dehydrogenases (IDH3), α-ketoglutarate dehydrogenase complex (αKGDH), branched-chain keto-acid dehydrogenase complex (BCKDH), glutamate dehydrogenase (GDH), malate dehydrogenase (MDH2), $NADP^+$-linked isocitrate dehydrogenase (IDH2), malic enzyme (ME), hydroxyacyl CoA (HADHA)), and GOT2 activity, although there was an upward trend for MDH2 activity in the Doxo group (Fig. 5*B*).

ETS supercomplexes, ATP synthase content, and mitochondrial iron content are unaltered following doxorubicin treatment

Using isolated mitochondria prepared from PBS- and Doxo-treated mice, blue native PAGE experiments were carried out to quantify the combined content of the mitochondrial supercomplexes $I + III_2 + IV_2$, $I + III_2 + IV_1$, and $I + III_2 + II_n$, as well as CV. Exposure to Doxo did not alter the skeletal muscle content

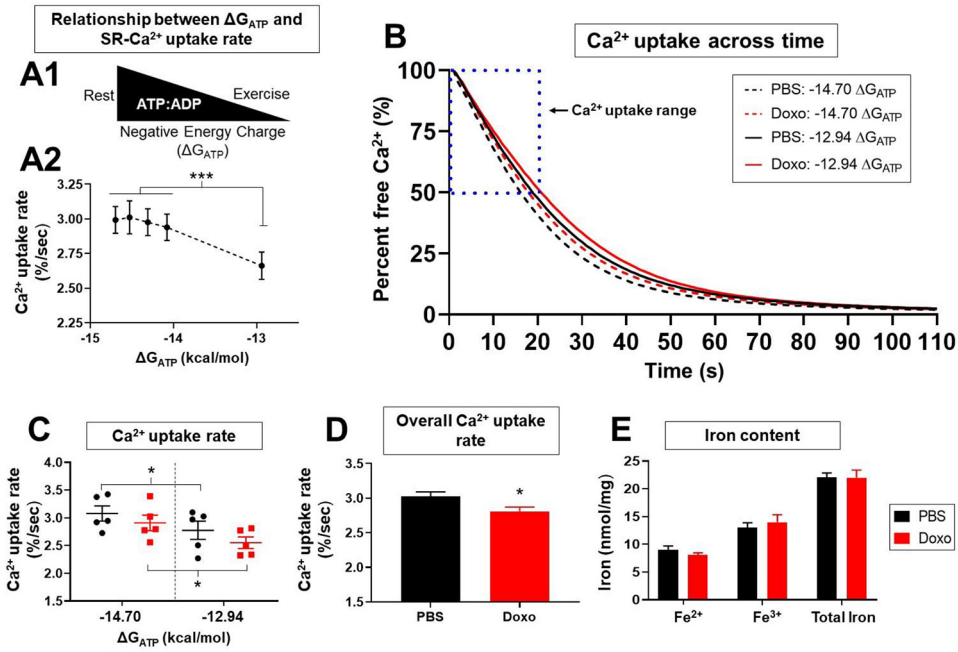

Figure 3. Doxorubicin reduces sarcoplasmic reticulum calcium uptake. *A1*, graphic illustrating the relationship between shifts in the ATP/ADP ratio and ΔG_{ATP}. *A2*, PBS and Doxo Ca^{2+} uptake rates data combined and plotted against ΔG_{ATP}, demonstrating SR–Ca^{2+} uptake rate sensitivity to changes in ΔG_{ATP}. *B*, tracing of percentage of Ca^{2+} uptake across time by isolated SR under different free energies of ATP hydrolysis (ΔG_{ATP}). The *box* outlines the data used to calculate Ca^{2+} uptake rates. *C*, Ca^{2+} uptake rate in isolated SR at high (−14.70) and low (−12.94) negative ΔG_{ATP}. *D*, overall Ca^{2+} uptake rate averaged across all five ΔG_{ATP} tested. *E*, ferrous (Fe^{2+}), ferric (Fe^{3+}), and total iron (Fe^{2+} + Fe^{3+}) content of gastrocnemius muscles from PBS- and Doxo-treated mice. For all measures: PBS, $n = 5$; and Doxo, $n = 5$. *, $p < 0.05$; ***, $p < 0.001$. The data are means ± S.E.

of either mitochondrial supercomplexes or CV (Fig. 5, *C–E*). Finally, iron content was similar in mitochondria isolated from PBS- and Doxo-treated mice (Fig. 5*F*).

Soleus muscle more susceptible to doxorubicin-induced mitochondrial respiratory deficits

Mitochondrial JO_2 was reduced independent of ΔG_{ATP} in soleus permeabilized muscle fiber bundles (PMFBs) energized with G/M but remained unchanged when energized with R/S (Fig. 6, *A* and *B*). Respiration rates were unchanged in EDL fiber bundles regardless of substrate condition (Fig. 6, *A* and *B*). Together, these data suggest a divergent susceptibility to Doxo-induced mitochondrial defects between EDL and soleus muscle, with the primary deficit localized to complex I of the ETS. Maximal complex IV JO_2 was unhindered in the EDL and soleus (Fig. 6*C*), suggesting no loss of functional complex IV units and that any intrinsic lesions are not sensitive to ΔG_{ATP} fluxes outside the physiological range.

Discussion

Loss of skeletal muscle quality is a consistent feature of doxorubicin myotoxicity. In the current study, this was manifest as impaired muscle force, fatigue, and contractile properties, including reduced rates or SR Ca^{2+} uptake, as well as the development of a mitochondriopathy. The extent of body mass lost in the current study was appreciable to that previously reported using a similar study design (9, 14), causing a relative increase in EDL and soleus muscle mass. Similar individual fiber CSAs between groups confirm that this was an artifact of significant loss of body mass and not hypertrophy. The collective muscle anthropometric and force data from the current study find that reductions in muscle performance precede the onset of any measurable muscle atrophy. As such, muscle atrophy following doxorubicin exposure is likely a consequence rather than a cause of the doxorubicin-induced myopathy. The significant reduction in EDL and soleus specific force agrees with previous studies showing EDL contractile decline in the absence of muscle atrophy markers (8, 9) and provides evidence that acute doxorubicin exposure diminishes EDL and soleus contractile function prior to the onset of measurable muscle atrophy. Additionally, EDL and soleus contractile decline was not associated with muscle fiber–type shifts, which were unaffected by Doxo treatment.

Both the EDL and soleus were impacted, with the extent of impairment different across the muscles, demonstrating a degree of muscle or fiber-type specificity to doxorubicin myotoxicity. The main fiber type–specific differences were the decline in EDL fatigue resistance and the increase in soleus half-relaxation time. That the EDL demonstrated a sharp decline in fatigue resistance and the soleus did not may be due to their respective myofiber type characteristics. For example, the soleus possesses a significantly greater fatigue resistance compared with the EDL (21). Doxorubicin has previously been shown to impair soleus fatigue resistance 5 days post-treatment in rat soleus (8, 12), but not EDL (12), using a more strenuous fatigue protocol compared with the current study. Doxorubicin-induced increases in fatigability are therefore specific to the study time course, species, and fatigue protocol employed. The soleus-specific increase in half-relaxation time may be due to differences in SR machinery compared with the EDL. Contractile kinetics are substantially faster in the EDL compared with

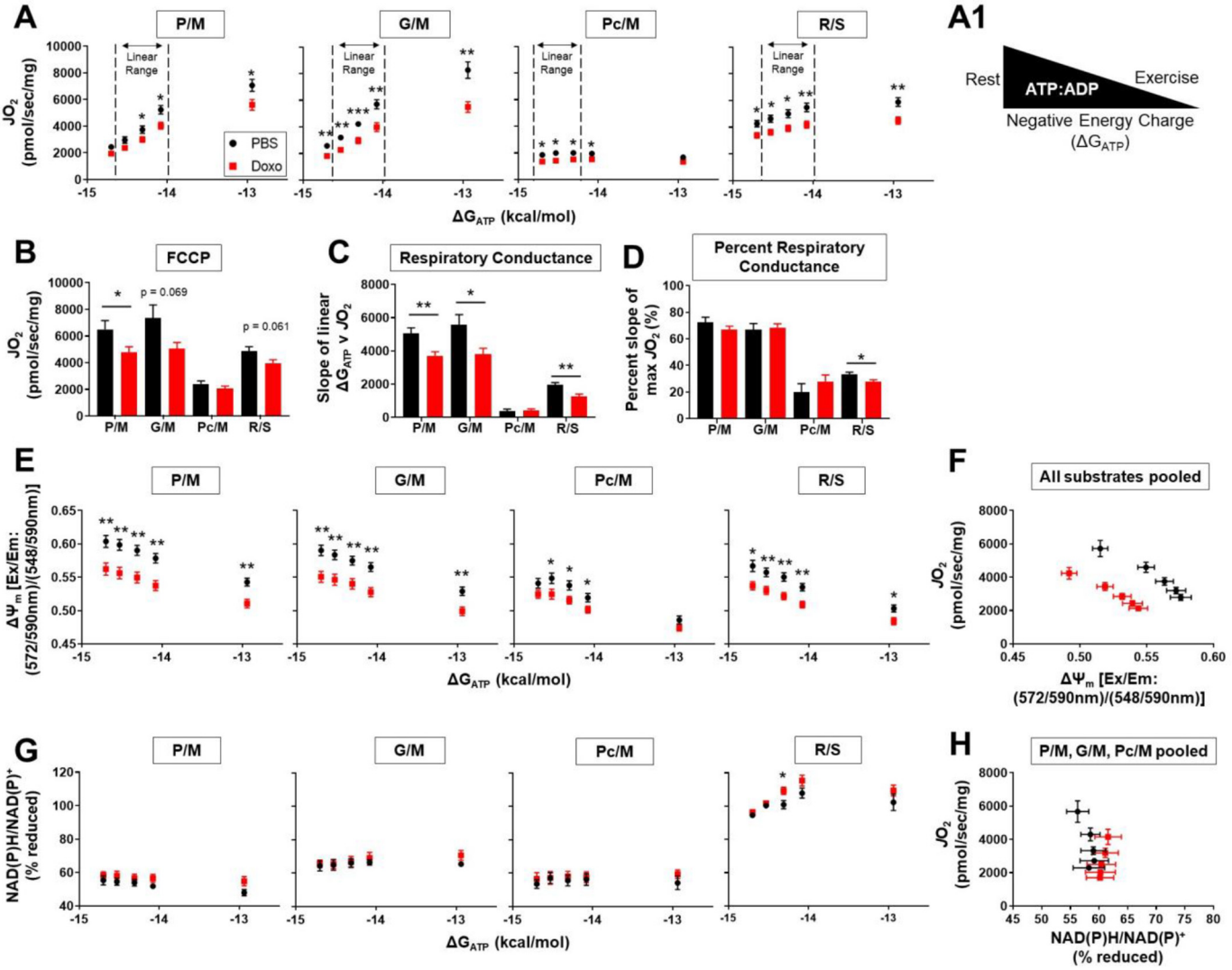

Figure 4. Multiplexed assay platform showing respiratory, membrane potential, and NAD(P)H/NAD(P)$^+$ fluxes in response to changing mitochondrial free energies following doxorubicin treatment. *A*, *E*, and *G*, relationship between mitochondrial oxygen consumption (JO_2) (*A*), membrane potential ($\Delta\Psi_m$) (*E*), and redox status (NAD(P)H/NAD(P)$^+$) (*G*) *versus* ATP free energy (ΔG_{ATP}) in isolated mitochondria energized with pyruvate/malate (P/M), glutamate/malate (G/M), palmitoyl-carnitine/malate (Pc/M), and rotenone/succinate (R/S). *A1*, graphic illustrating the relationship between shifts in the ATP/ADP ratio and ΔG_{ATP}. *B*, JO_2 following addition of the uncoupling agent, FCCP. *C*, respiratory conductance calculated from the slopes of the linear range (*dashed lines* in *A*) of JO_2 v ΔG_{ATP}. *D*, respiratory conductance normalized to max JO_2. *F*, data from all substrates was pooled to provide an overview of the relationship between JO_2 and $\Delta\Psi_m$. *H*, data from P/M, G/M, and Pc/M was pooled to provide an overview of the relationship between JO_2 and NAD(P)H/NAD(P)$^+$. For all measures: PBS, $n = 8$; and Doxo, $n = 8$. *, $p < 0.05$; **, $p < 0.01$. The data are means ± S.E.

the soleus, aided by greater calsequestrin content (22) and SERCA activity (23), which may protect against doxorubicin-related damage or inhibition. Increases in half-relaxation time were limited to low frequency stimulation (10 Hz), suggesting that any doxorubicin impairment or inhibition was mild under the acute dose and time course assessed. The underlying causes of changes in half-relaxation are likely the noted reductions in SR-dependent Ca^{2+} uptake following doxorubicin treatment.

We assessed Ca^{2+} uptake in isolated SR, with a novel modification. Similar to our mitochondrial assays, we employed a CK clamp, allowing us to manipulate the free energy of ATP hydrolysis and measure its impact on SR-dependent Ca^{2+} uptake. This approach allows us to connect components that regulate skeletal muscle contractile function with cellular energetic status, and potentially mitochondrial function, which are responsible for maintaining cellular energetic homeostasis. Our data support those of previous investigations demonstrating doxorubicin-induced reductions in Ca^{2+} uptake (11, 24, 25). Reductions in Ca^{2+} uptake were found across the spectra of ΔG_{ATP} tested, indicating that the mechanism of doxorubicin impairment was not related to abnormal SERCA sensitivity to cellular ΔG_{ATP}. Oxidation of thiol groups caused by elevated ROS has been proposed as a potential mechanism of SERCA inhibition (24) but remains unresolved based on the mix of positive (24, 26) and negative (11) anti-oxidant supplementation studies. Impaired Ca^{2+} uptake via the SR would be expected to be most pronounced under high-frequency tetanic contractions, such as those in which EDL specific force was significantly reduced. Meanwhile, the soleus demonstrated reduced specific force across all but the lowest frequency stimulations. The differences in EDL and soleus muscle response may be due to the

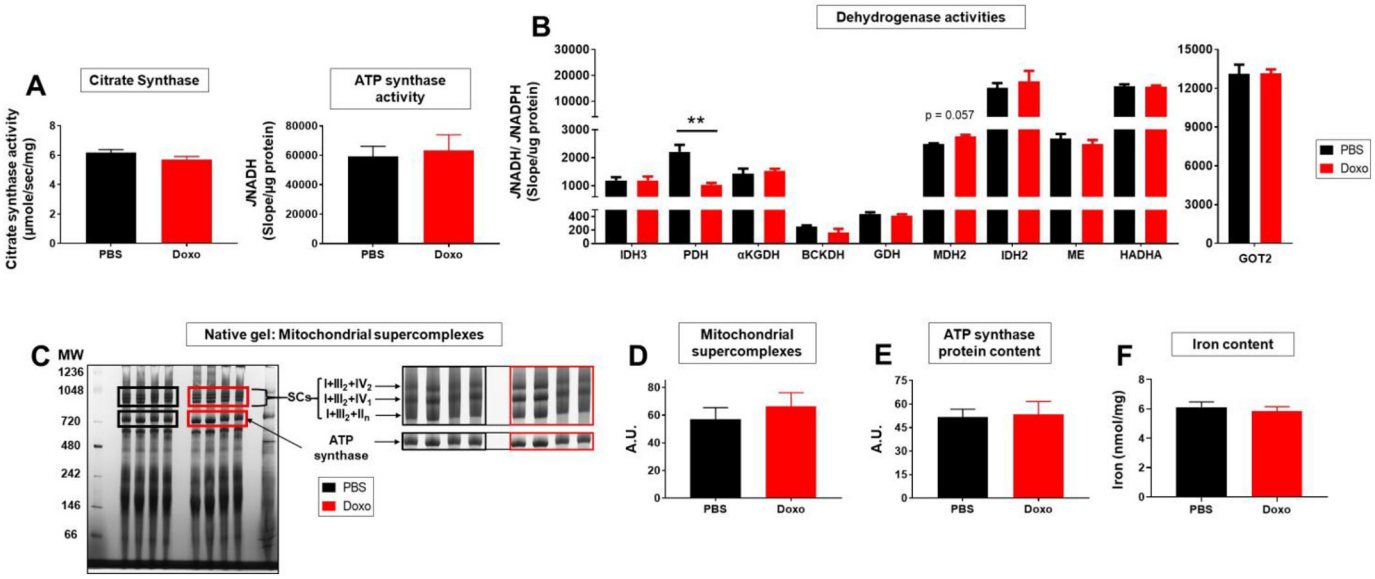

Figure 5. Dehydrogenase flux capacity and mitochondrial content of subunit supercomplexes and ATP synthase. *A*, citrate synthase and ATP synthase (CV) activity rates. *B*, enzyme activity rates (*J*NADH/*J*NADPH) of mitochondrial dehydrogenases. *C*, whole blue native PAGE gel and *magnified inset* showing mitochondrial supercomplex and ATP synthase protein content. *D* and *E*, doxorubicin did not alter the protein content of mitochondrial supercomplexes I + III_2 + IV_2, I + III_2 + IV_1, and I + III_2 + II_n (*D*) or ATP synthase (*E*). *F*, total iron (Fe^{2+} + Fe^{3+}) content of isolated mitochondria from PBS-treated ($n = 4$) and Doxo-treated ($n = 3$) mice was similar between groups. For all measures: PBS, $n = 4$; and Doxo, $n = 4$ unless otherwise stated. **, $p < 0.01$. The data are means ± S.E.

significantly higher calsequestrin content (22) and SERCA activity (23) in the EDL compared with the soleus.

A further explanation may be the occurrence of dysregulated skeletal muscle mitochondria in response to doxorubicin exposure. Muscle contractile performance and mitochondria are integrated through a series of phosphotransfer reactions mediated by creatine kinase and adenylate kinase (27, 28). These coupled reactions relay changes in adenylate flux across the cell, providing a means of energetic communication between the SR and mitochondria to regulate Ca^{2+} release and reuptake and ATP synthesis and hydrolysis (15–17). The bidirectional nature of this communication means that altered mitochondrial function may impact Ca^{2+} handling and consequently muscle performance. Findings from the current study in which doxorubicin-induced mitochondriopathy was associated with reduced Ca^{2+} uptake and contractile dysfunction support such a mechanism. Ca^{2+} uptake measures in the current study were made in isolated SR and thus in the absence of mitochondrial coupling. However, reduced Ca^{2+} uptake has previously been reported in permeabilized muscle fiber bundles prepared from doxorubicin treated rat gastrocnemius muscle in which SR-mitochondrial excitation coupling remained intact (14). Indeed, impaired intracellular Ca^{2+} handling has previously been found in models of skeletal muscle mitochondrial dysregulation (16, 29). Comparison of mitochondrial respiration in PMFBs found complex I–dependent JO_2 reductions in the soleus following Doxo, but not the EDL. Complex II was unaffected across all ΔG_{ATP} in both muscles, and maximal complex IV JO_2 was similarly unaltered. These data imply an increased susceptibility within type I/IIa fiber type–rich muscles to complex I-dependent lesions following acute doxorubicin exposure. Whether and to what extent this contributes to contractile dysfunction in the soleus is unclear. It may be anticipated that if doxorubicin-related muscle dysfunction is the result of impaired mitochondrial function, muscles in which energetics were most dependent on mitochondria, such as the soleus, would show a more debilitating phenotype. A comparison of EDL and soleus contractile data, which do not show drastic differences, suggests this may not be the case in acute doxorubicin exposure, but a contributing factor cannot be ruled out.

Mitochondria isolated from skeletal muscle 72 h after systemic doxorubicin exposure showed a pronounced decline in JO_2. The substrate-independent nature of the respiratory decline indicates that the source of respiratory limitation is likely not caused by dehydrogenase impairments, nor is it limited to CI (P/M, G/M, and Pc/M) or CII (R/S) exclusively. Furthermore, that JO_2 remained lower with the addition of FCCP demonstrates a reduction in the maximal respiratory capacity of the mitochondria following doxorubicin treatment. Together, these data suggest the presence of biochemical lesions within the ETS. Conflicting R/S JO_2 data between PMFBs and isolated mitochondria likely reflects differential responses to doxorubicin exposure across different muscles groups or potential differences in methodology. Respiratory sensitivity, which measures the responsiveness of mitochondria to changes in ΔG_{ATP}, was also lower in the Doxo group, although with the exception of R/S, this reduction was in line with the overall depression in absolute respiration. As such, the respiratory defect is likely not caused by intrinsic limitations to any one ETS component but rather the result of fewer functional respiratory complexes and/or a multiplexed lesion across the ETS. In the case of CII, however, normalized respiratory conductance remained suppressed, implying that a CII-intrinsic limitation may be present. Quantification of both mitochondrial supercomplexes and ATP synthase imply that neither depletion of ETS components or ETS complex– complex inter-

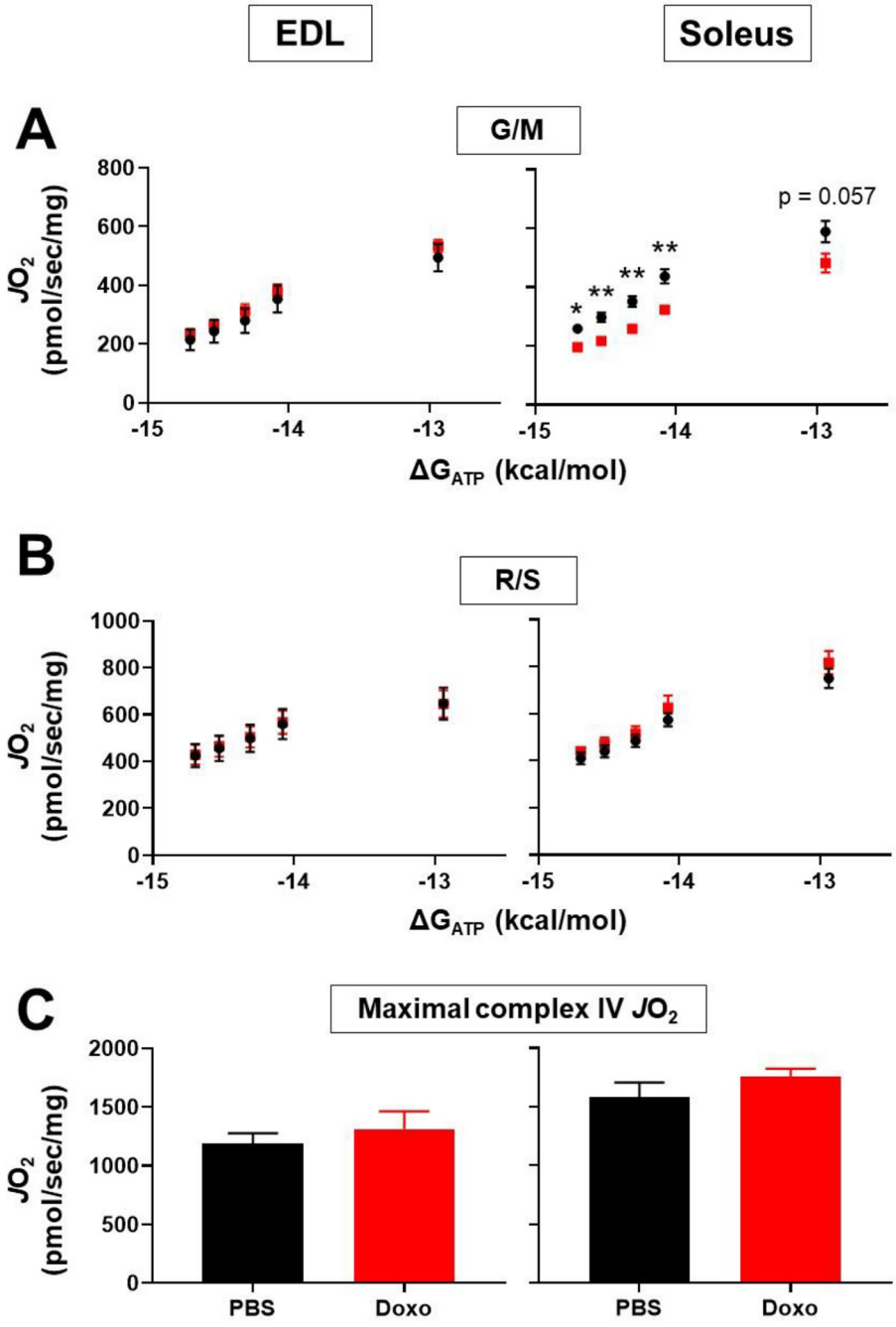

Figure 6. Respiratory flux changes between EDL and soleus muscle in response to doxorubicin. *A* and *B*, relationship between mitochondrial oxygen consumption and changes in ATP free energy (ΔG_{ATP}) measured in EDL and soleus PMFBs energized with glutamate/malate (G/M) (for EDL: PBS, $n = 3$; and Doxo, $n = 3$; for soleus: PBS, $n = 9$; and Doxo, $n = 6$) (*A*) and rotenone/succinate (R/S) (for EDL: PBS, $n = 3$; and Doxo, $n = 3$; for soleus: PBS, $n = 8$; and Doxo, $n = 7$) (*B*). *C*, maximal complex IV oxygen consumption in EDL and soleus PMFBs (for EDL: PBS, $n = 6$; and Doxo, $n = 6$; for soleus: PBS, $n = 6$; and Doxo, $n = 6$). *, $p < 0.05$; **, $p < 0.01$. The data are means ± S.E.

actions are the underlying causes of doxorubicin-induced mitochondriopathy. That said, future studies will require thorough interrogation of the respiratory proteome to definitively rule out ETS complex depletion as the cause of Doxo-mediated bioenergetic decline.

Similar to JO_2, we found substrate-independent reductions in membrane potential following doxorubicin treatment. Such a depolarization effect implies that Doxo either impairs proton pumping or accelerates proton leak, both of which impair the mitochondrion's ability to maintain membrane potential. When considered in the context of respiration, by plotting $\Delta\Psi_m$ against JO_2, the Doxo group exhibit a distinct leftward shift relative to the PBS group. This shift is inconsistent with the depolarization effect being caused by proton leak (*i.e.* "uncoupling") and thus supports that the respiratory defect resides in the ETS. To further interrogate the maintenance of mitochondrial free energy following doxorubicin exposure, we measured the NAD(P)H/$NAD(P)^+$ reduction state. Similar NAD(P)H/$NAD(P)^+$ levels were observed for both groups under P/M, G/M, and Pc/M energized conditions. Plotting JO_2 against

pooled NAD(P)H/NAD(P)$^+$ revealed no shift in the Doxo group, indicating that the activity of the matrix dehydrogenases were not rate-limiting and therefore not the cause of depressed JO_2 and $\Delta\Psi_m$. Interestingly, NAD(P)H/NAD(P)$^+$ was hyperreduced in the presence of R/S. Although the molecular mechanism underpinning this observation remains to be determined, a similar phenotype was recently reported in cardiac mitochondria from the mitochondrial mutator mouse (30).

Unique among the dehydrogenases tested was PDH, which showed a greater than 50% reduction in maximal activity following doxorubicin treatment. Phosphorylation via pyruvate dehydrogenase kinase (PDK) provides a potent inhibitory effect on PDH. Increased PDK expression in response to doxorubicin treatment has previously been shown in mouse skeletal muscle (19) and cardiomyocytes (31). Although subsequent reductions in PDH activity were only found in cardiomyocytes, discrepancies in PDH activity are likely the result of differences in models, doxorubicin doses, assays, and the use of whole-tissue/cell homogenates compared with isolated mitochondrial homogenates. Nevertheless, elevated PDK expression in doxorubicin-exposed cardiomyocytes was associated with increased PDH phosphorylation (31). In light of this, it is likely that reduced PDH activity in the current study was the result of PDK-regulated phosphorylation of PDH. The absence of a difference in NAD(P)H/NAD(P)$^+$ under P/M conditions suggests that any phosphorylation-mediated declines in PDH activity were reversed in intact mitochondria upon energization with excess pyruvate under physiological ATP free energy (32, 33). In addition to dehydrogenase activity, we measured the activity and protein content of ATP synthase (CV). The similar activities and protein content of ATP synthase between PBS and Doxo groups indicate that the doxorubicin-associated defects in mitochondrial respiration are upstream of CV. These data in conjunction with those of the multiplexed assay reveal that doxorubicin causes lesions in the ETS. The primary candidates of which are CI, CII, CIII, and/or CIV. This concept is summarized in the Fig. 7 diagnostic tree. Comparison with muscle fiber JO_2 data suggests that the major lesions reside within complex I and are most prevalent within oxidative muscle fiber groups. Whether the source of ETS limitation involves the stoichiometry of the individual complexes and/or post-translational control (*e.g.* cysteine oxidation) requires further investigation.

It has been proposed that the mechanism underlying the decline in muscle and mitochondrial quality is the excessive production of ROS caused by doxorubicin cycling. Briefly, the quinone moiety, aglycone, within doxorubicin produces a semiquinone through a readily reversible reaction, via the transfer of an electron from O_2, in turn producing superoxide and subsequently H_2O_2 (34, 35). When in the vicinity of heavy metals such as iron, which as a curious by-product of doxorubicin exposure accumulates in mitochondria (36), is converted to potent hydroxyl radicals (37, 38). Extensive oxidant damage may trigger the release of cytochrome *c* from mitochondria and subsequent activation of proteases, leading to the onset of atrophy (19, 39) and ultimately the loss of skeletal muscle quality. Doxorubicin not only disrupts iron homeostasis through redox cycling and iron accumulation but can interact directly with iron to form a Doxo–iron complex (36, 38, 40). It is interesting therefore that all four ETS complex candidates for doxorubicin-induced lesion loci contain heme and/or iron–sulfur clusters, which are required for electron transport (41). Interference with iron homeostasis across complexes I–IV could potentially inhibit electron flow and reduce JO_2 and Ψ_m. Iron content analysis revealed that neither cellular nor mitochondrial free iron accumulation was a contributing factor to the myopathy and mitochondriopathy developed herein in response to acute doxorubicin exposure. That said, transgenic and pharmacological interventions aimed at reducing mitochondrial iron content in mice were found to alleviate and reverse doxorubicin-induced cardiotoxicity (36), suggesting that iron accumulation may be a contributing factor in long-term, multidose doxorubicin treatments but not short-term doxorubicin treatments. Future work will be required to determine whether doxorubicin-mediated impairments in bioenergetic efficiency proceed through a direct interaction between doxorubicin and respiratory complex iron-containing prosthetic groups.

Experimental procedures

Animal use and care

The mice were purchased from the Jackson Laboratory and housed in a temperature (22 °C) and 12 h light/dark cycle-controlled facility with *ad libitum* access to food and water. The mice were euthanized via isoflurane overdose and cervical dislocation. All animal procedures and usage were approved by the Institutional Review Committee at East Carolina University (animal usage protocol no. Q332a). Animal care complied with the Guide for the Care and Use of Laboratory Animals, Institute of Laboratory Animal Resources, Commission on Life Sciences, National Research Council (42).

Procedures

A total of 41 C57BL/6NJ male mice, aged 10–24 weeks were euthanized during the study. The mice received an intraperitoneal injection of either 1× PBS or Doxo at a clinically equivalent dose of 20 mg/kg body mass based on the established Freireich conversion factor (43). PBS and Doxo treatments were administered in equal volumes. Following injections, the mice were monitored daily and then euthanized 72 h postinjection. The mice were weighed pre- and postinjection for calculation of injection volume and changes in body. EDL and soleus muscles were tied and extracted for isometric force measures and muscle fiber CSA. Quadracep, gastrocnemius, and tibialis anterior (TA) muscles were extracted for mitochondrial isolation. Mitochondria were isolated into three pellets, an intact pellet for conductance measures (respiration, membrane potential, and redox), a homogenate for enzyme activity assays, and an intact pellet for assessment of supercomplexes. Finally, mitochondrial respiration was measured in PMFBs prepared from EDL and soleus muscles to compare tissue specific differences.

Muscle fiber size and type

Muscle fiber CSA was measured in EDL and soleus muscles (PBS, $n = 4$; Doxo, $n = 4$), as described previously (21). Images of muscle cross-sections were taken by a blinded investigator

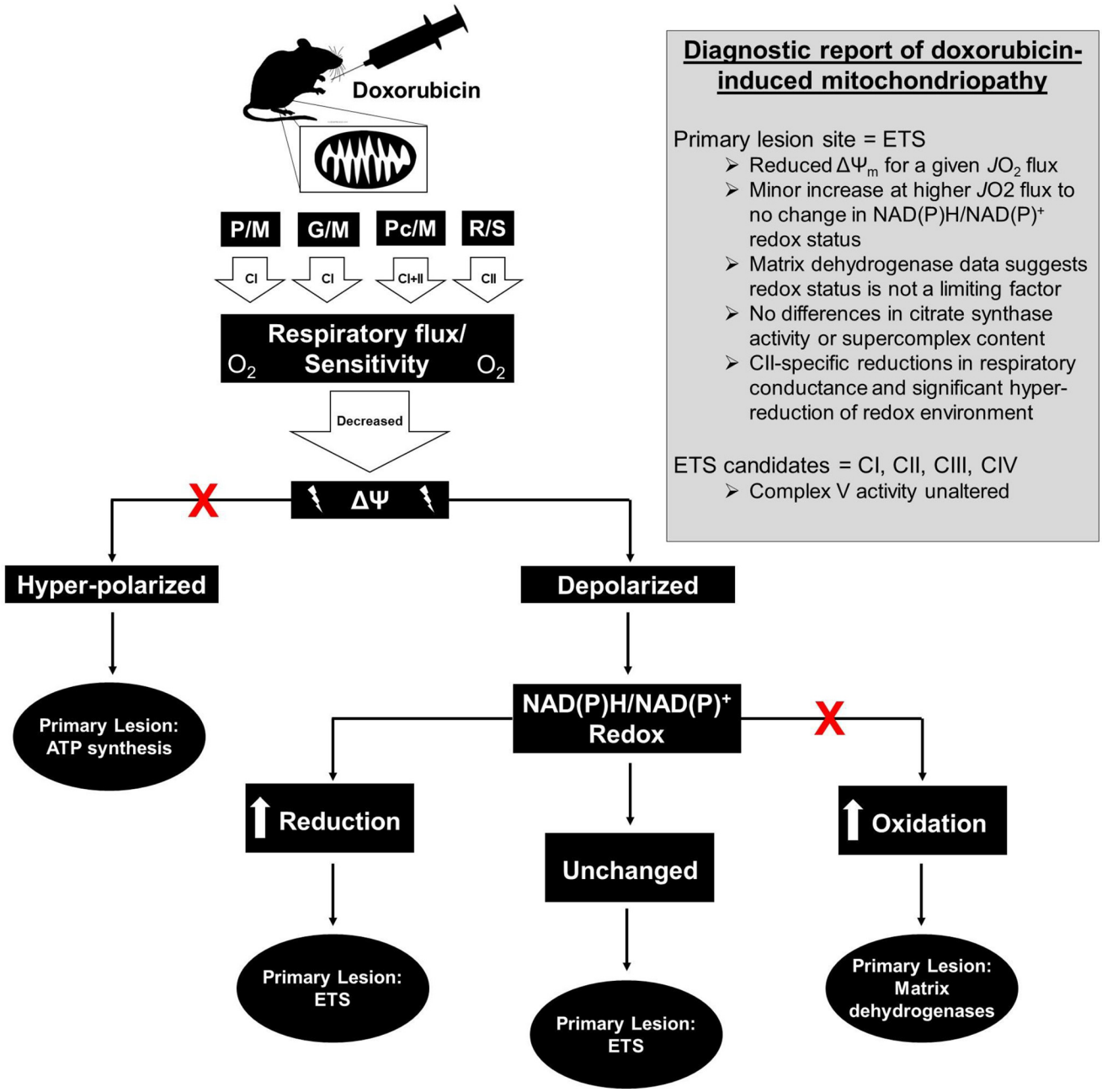

Figure 7. Summary diagnostic workflow of mitochondria from doxorubicin-treated mice. The summary displays the analytical process of determining potential lesion targets. Overlaying the findings of the current study onto the workflow reveals that decreased respiratory flux, in conjunction with depolarized membrane potential and reduced/no change in NAD(P)H/NAD(P)$^+$ redox state, is symptomatic of lesions to the ETS. Specific targets and supporting evidence are listed in the *diagnostic report box*.

from six different locations across the belly of the muscle section and were probed with an anti-dystrophin primary antibody (Rb-9024; Thermo Fisher). Dystrophin protein was stained with a secondary fluorescent 647 probe (A-21244; Thermo Fisher). Muscle fiber type was assessed as previously described (21). Stained cross-sections were imaged using an EVOS FL auto microscope and accompanying software (Life Technologies, Inc.). CSA was assessed using ImageJ (National Institutes of Health) as previously described (44). The images were coded and randomized to allow for blinded analyses.

Muscle force production

Isometric force production and fatigue were assessed *in vitro* for EDL and soleus muscle (PBS, $n = 8$; Doxo, $n = 9$), as previously described (21) with slight modifications. Briefly, EDL and soleus muscles were equilibrated in oxygenated Krebs buffer at room temperature for 10 min prior to setting optimal resting tension. Force–frequency curves were generated by stimulating muscles at 10, 20, 40, 60, 80, 100, and 120 Hz every 60 s. To ensure maximal stimulation, an optimal voltage of 20 V was determined for EDL and soleus muscles prior to experiments. Following the force–frequency curve, the muscles were allowed

to rest for 60 s before a 150-contraction fatigue resistance protocol was initiated. The protocol stimulated muscles at 30 Hz every 2 s for 300 s. Upon completion of the protocol, optimal muscle length was measured, and muscles were blotted, dried, and weighed. Absolute muscle force data (mN) were converted to specific force (N/cm^2) using an equation for the estimation of physiological CSA (45).

Sarcoplasmic reticulum calcium uptake

SR was isolated from PBS-treated ($n = 5$) and Doxo-treated ($n = 5$) mice as previously described (46), with modifications. An enriched SR fraction was isolated from quadriceps, gastrocnemius, and TA muscles placed in 10 ml of ice-cold isolation buffer (20 mM HEPES, 0.2% sodium azide, 0.2 mM phenylmethylsulfonyl fluoride, pH 6.8). The muscles were chopped prior to mechanical homogenization with a Polytron homogenizer. The samples were centrifuged at 8,000 × *g* for 15 min at 4 °C to remove debris. Supernatant was removed and filtered through a 100-μm nylon filter into a clean tube. KCl was added to a final concentration of 600 mM to dissolve cytoskeleton proteins. The samples were centrifuged at 12,000 × *g* for 45 min at 4 °C. Supernatent was discarded, and pellets were dislodged via a rubber policeman into storage buffer (20 mM HEPES, 0.2% sodium azide, 0.2 mM phenylmethylsulfonyl fluoride, 300 mM sucrose, 150 mM KCl, pH 6.8). Protein concentration was determined using a BCA assay (Pierce BCA protein assay kit; Thermo Fisher).

Oxolate-supported Ca^{2+} uptake was measured using the duel emission fluorescent probe, Indo-1, as previously described (46, 47), with modifications. Measurements were made at 1-s intervals, and changes in the 468:402 emission ratio were normalized to the percentage change for the calculation of Ca^{2+} uptake rates. All measures were made in duplicate, and the purity of each SR isolate was confirmed by an additional assay run including 50 μM of the sarco/endoplasmic reticulum Ca^{2+}-ATPase (SERCA) inhibitor cyclopiazonic acid.

Measurements were made in 200 μl of Indo-1 assay buffer (100 mM KCl, 20 mM HEPES, 5 mM oxalate, 1 mM $MgCl_2$, 5 mM ATP, 5 mM creatine, 20 μg/ml CK, 1.5 μM Indo-1, pH 7.0) using 7.5 μg of isolated SR protein. Assay buffer was supplemented with 1, 6, 11, 16, and 21 mM PCr to modulate the free energy of ATP hydrolysis ($\Delta G'_{ATP}$). Once the 468:402 emission ratio had plateaued, 40 μM $CaCl_2$ was added to initiate SR Ca^{2+} uptake.

$\Delta G'_{ATP}$ was calculated for each PCr step to account for shifts in ionic strength and free magnesium, as previously described (48, 49). $\Delta G'_{ATP}$ was calculated using the formula below,

$$\Delta G'\ ATP = \Delta G'^{\circ}\ ATP + RT \ln \frac{[Cr][P_i]}{[PCr][K'_{CK}]}$$

where $\Delta G'^{\circ}_{ATP}$ is the standard apparent transformed Gibbs energy (at a specified pH, ionic strength, free magnesium, and pressure), R is the gas constant (8.3145 J/kmol), and T is the temperature in kelvin (310.15). $\Delta G'_{ATP}$ values were determined using an online tool (https://dmpio.github.io/bioenergetic-calculators/) (50).[3]

[3] Please note that the JBC is not responsible for the long-term archiving and maintenance of this site or any other third party hosted site.

Respiratory conductance was determined by plotting the free energy of ATP hydrolysis ($\Delta G'_{ATP}$) at each PCr titration step against oxygen consumption rates (JO_2). $\Delta G'_{ATP}$ was calculated as described above.

Isolation of skeletal muscle mitochondria

Mitochondria were isolated from the quadriceps, gastrocnemius, and TA muscles via differential centrifugation, as previously described (50). Mitochondria were isolated in three buffers: buffer A (PBS and 10 mM EDTA at pH 7.4); buffer B (50 mM MOPS, 100 mM KCl, 1 mM EGTA, 5 mM $MgSO_4$); and buffer C (buffer B and 2 g/liter BSA). The muscles were placed in ice-cold buffer A, minced, and then digested in 0.05% trypsin for 5 min. Trypsin was removed via centrifugation at 300 × *g* for 5 min at 4 °C. Muscle pellets were homogenized in buffer C using a Teflon pestle and borosilicate glass vessel and then centrifuged at 600 × *g* for 10 min at 4 °C. Supernatants were passed through a double layer of gauze and centrifuged at 10,000 × *g* for 10 min at 4 °C. Mitochondrial pellets were suspended in 1.4 ml of buffer B and divided into suspensions of 1 ml (pellet 1), 200 μl (pellet 2), and 200 μl (pellet 3) and centrifuged at 10,000 × *g* for 10 min at 4 °C. Pellet 1 was suspended in 100 μl of buffer B for conductance measures, pellet 2 was suspended in 50 μl of buffer B supplemented with protease inhibitors for enzyme activity assays and flash frozen, and pellet 3 was flash frozen for mitochondrial supercomplex analysis, respectively. Protein concentrations were determined using a BCA assay.

Isolated mitochondrial respiratory control (JO_2)

High resolution respirometry measures were conducted at 37 °C in 2 ml of assay buffer using the Oroboros Oxygraph-2K (Oroboros Instruments), as previously described (51). All respiratory assays were run in buffer D supplemented with 5 mM creatine, 5 mM ATP, 1 mM PCr, and 20 units/ml CK. The substrate conditions tested were 5 mM pyruvate and 2.5 mM malate (P/M), 10 mM glutamate and 2.5 mM malate (G/M), 16 μM palmitoyl-carnitine and 2.5 mM malate (Pc/M), and 5 μM rotenone and 10 mM succinate (R/S). A total of 40 μg of mitochondrial protein was used for each of the P/M, G/M, and R/S conditions, and 75 μg of mitochondrial protein was used for the Pc/M condition. Respiratory control was assessed through sequential additions of PCr to final concentrations of 6, 11, 16, and 21 mM before addition of 5 μM FCCP and 10 μM cytochrome *c*.

Mitochondrial membrane potential and redox state

Membrane potential ($\Delta\Psi_m$) and redox state (NAD(P)H/$NAD(P)^+$) measures were made simultaneously at 37 °C in 0.2 ml of assay buffer using a QuantaMaster spectrofluorometer. The assays were run in buffer D supplemented with 5 mM ATP, 1 mM PCr, 20 units/ml CK, and 0.2 μM tetramethylrhodamine, methyl ester. Isolated mitochondria (0.1 mg/ml) were added to cuvettes, followed by P/M, G/M, Pc/M, and R/S substrate conditions (as used in respiratory control experiments). Sequential additions of PCr were made to final concentrations of 6, 11, 16, and 21 mM. Following PCr titrations, 10 mM cyanide and 0.03 mg/ml alamethicin were added in sequence to induce a state of 100 and 0% reduction, respectively. $\Delta\Psi$ was determined via

tetramethylrhodamine, methyl ester fluorescence using the excitation/emission parameters: excitation/emission (572/590 nm)/(551/590 nm), as previously described (51). NAD(P)H/$NAD(P)^+$ was calculated via autofluorescence using the excitation/emission parameters 340 nm/450 nm. NAD(P)H/$NAD(P)^+$ was calculated for each $\Delta G'_{ATP}$ value and expressed as a percentage reduction using the formula below, where F is the fluorescence signal (340 nm/450 nm).

$$\%\ reduction = \frac{(F - F_{0\%})}{(F_{100\%} - F_{0\%})}$$

Citrate synthase activity assay

Protein content of mitochondrial homogenates were assessed using a BCA assay. Citrate synthase activity was determined using a commercially available citrate synthase assay kit (catalog no. CS0720; Millipore–Sigma). Citrate synthase activity was determined using the manufacturer's instructions.

Enzyme activity assays

All assays were completed as previously described (50) using isolated mitochondrial homogenates. Enzyme activities were determined based on rates or NADH/NADPH production or oxidation measured via autofluorescence (excitation/emission 340/450). The assays were run in 96-well plates using 200 μl of buffer and 2–60 μg/well mitochondrial protein. The fluorescence values were plotted over time, and the slope for the linear portion of the curve was calculated. Slope values were background-corrected and normalized to total number of micrograms of mitochondrial protein loaded per assay.

ATP synthase—The activity of ATP synthase (complex V) was measured via NADH oxidation using buffer D, supplemented with 0.005 mM rotenone, 0.2 mM NADH, 10 units/ml lactate dehydrogenase, and 5 mM phosphoenoyl pyruvate. The assay was initiated with the addition of 5 mM ATP.

Dehydrogenases—The assays were performed to determine the activity of the dehydrogenases isocitrate (IDH3: NAD-linked), PDH complex, αKGDH, BCKDH, GDH, MDH2, isocitrate dehydrogenase (IDH2: $NADP^+$), ME, and HADHA. The following assays were performed using buffer C with the addition of dehydrogenase-specific supplements. IDH2 and ME was supplemented with 0.005 mM rotenone and 2 mM $NADP^+$. IDH3, GDH, and MDH2 were supplemented with 0.005 mM rotenone and 2 mM NAD^+. PDH, αKGDH, and BCKDH were supplemented with 0.005 mM rotenone, 2 mM NAD^+, 0.1 mM cofactors CoA, and 0.3 mM thiamine pyrophosphate. The activity of HADHA was measured using buffer D, supplemented with 0.005 mM rotenone and 0.2 mM NADH with 0.2 mM acetoacetyl-CoA added to initiate the reaction.

GOT2—The activity of aspartate aminotransferase (GOT2) was measured via NADH oxidation using buffer E (20 mM HEPES, 100 mM KCl, 2.5 mM KH_2PO_4, 2.5 mM $MgCl_2$, and 1% glycerol, pH 8.0) supplemented with 200 mM aspartate, 0.1 mM pyridoxal 5-phosphate, 2 units/ml malate dehydrogenase, 0.005 mM rotenone, and 0.2 mM NADH. The assay was initiated with the addition of 10 mM α-ketoglutarate.

Blue native PAGE

Mitochondrial pellets were lysed in 1× native gel electrophoresis buffer (catalog no. BN2003; Thermo), supplemented with 10 mM nicotinomide, 1× protease inhibitor mixture, and 6% digitonin. Samples were incubated on ice for 20 min and centrifuged at 10,000 × g for 30 min at 4 °C. Protein content of supernatants were determined via BCA assay. The samples were supplemented with G-250 Coomassie additive (catalog no. BN2004; Thermo), and then 50 μg of mitochondrial protein was loading onto a 4–16% BisTris native gel (catalog no. BN1004; Thermo). Following electrophoresis, the proteins were fixed and destained in 40% methanol and 10% acetic acid overnight at room temperature.

Iron content

Iron levels were measured in gastrocnemius homogenates (PBS, $n = 7$; Doxo, $n = 5$) and a subset of isolated mitochondrial (PBS, $n = 4$; Doxo, $n = 3$) homogenates using a commercially available assay kit (catalog no. K390-100; Biovision) and in accordance with the manufacturer's instructions. For gastrocnemius homogenates, the ferrous (Fe^{2+}) form and total iron content were measured, allowing for the calculation of ferric iron (Fe^{3+}) by subtraction of Fe^{2+} from total iron. Because of the limited sample, only the total iron content was measured for isolated mitochondria. Measurements were made in 150 and 120 μg of gastrocnemius and mitochondrial homogenate protein, respectively.

Permeabilized muscle fiber bundle preparation

PMFBs were prepared from EDL and soleus muscle of PBS- and Doxo-treated animals 72 h post-treatment. Fiber bundles were prepared as previously described (52). Briefly, the muscles were excised and placed in ice-cold buffer X (7.23 mM K_2EGTA, 2.77 mM CaK_2EGTA, 20 mM imidazole, 20 mM taurine, 5.7 mM ATP, 14.3 mM phosphocreatine, 6.56 mM $MgCl_2{\cdot}6H_2O$, 50 mM MES, pH 7.1). Connective tissue and fat were removed, and fibers underwent mechanical separation using a dissecting microscope and microdissecting tweezers. Fiber bundles were permeabilized in buffer X containing 30 μg/ml saponin with continuous rotation for 30 min at 4 °C. Fiber bundles were then washed in buffer D (105 mM potassium MES, 30 mM KCl, 10 mM KH_2PO_4, 5 mM $MgCl_2{\cdot}6H_2O$, 0.5 g/liter BSA, 1 mM EGTA, pH 7.1) for 15 min with continuous rotation at 4 °C.

High-resolution respirometry in PMFBs

High-resolution respiratory measures were conducted as previously described (50), with minor modifications. Respiratory assays were conducted in buffer D, supplemented with 5 mM creatine, 5 mM ATP, 1 mM PCr, 2 units/ml CK, and 25 μM blebbistatin. Substrate conditions comprised of 10 mM glutamate and 2.5 mM malate (G/M) and 5 μM rotenone and 10 mM succinate (R/S). Respiratory control was assessed through sequential additions of PCr to final concentrations of 6, 11, 16, and 21 mM. The mitochondria were re-energized with the addition of 20 units/ml hexokinase and 10 mM glucose. Mitochondrial membrane integrity was confirmed by the addition of 10 μM cytochrome c before additions of 5 μM antimycin A, 2 mM

ascorbic acid, and 0.5 mM *N*,*N*,*N*′,*N*′-tetramethyl-*p*-phenylenediamine dihydrochloride to assess maximal complex IV respiration. PMFBs were washed in dH_2O, freeze-dried, and weighed. JO_2 was normalized to PMFB mass.

Statistical analyses

Differences between groups were determined using *t* tests with Welch's correction, Mann–Whitney U tests, and multiple *t* tests. Statistical analyses and figure generation were completed using GraphPad Prism (version 7.0). The α level was set at $\alpha = 0.05$. The data are presented as means ± S.E.

Author contributions—M. D. T., K. H. F.-W., and E. E. S. conceptualization; M. D. T., A. J. A., and N. P. B. data curation; M. D. T., A. J. A., K. H. F.-W., and E. E. S. formal analysis; M. D. T., K. H. F.-W., and E. E. S. investigation; M. D. T., K. H. F.-W., and E. E. S. visualization; M. D. T., K. H. F.-W., and E. E. S. methodology; M. D. T., K. H. F.-W., and E. E. S. writing-original draft; M. D. T., K. H. F.-W., and E. E. S. project administration; M. D. T., K. H. F.-W., and E. E. S. writing-review and editing; K. H. F.-W. and E. E. S. resources; K. H. F.-W. and E. E. S. supervision.

References

1. Olson, R. D., Li, X., Palade, P., Shadle, S. E., Mushlin, P. S., Gambliel, H. A., Fill, M., Boucek, R. J., Jr., and Cusack, B. J. (2000) Sarcoplasmic reticulum calcium release is stimulated and inhibited by daunorubicin and daunorubicinol. *Toxicol. Appl. Pharmacol.* **169,** 168–176 CrossRef Medline
2. Fabris, S., and MacLean, D. A. (2015) Skeletal muscle: an active compartment in the sequestering and metabolism of doxorubicin chemotherapy. *PLoS One* **10,** e0139070 CrossRef Medline
3. Gouspillou, G., Scheede-Bergdahl, C., Spendiff, S., Vuda, M., Meehan, B., Mlynarski, H., Archer-Lahlou, E., Sgarioto, N., Purves-Smith, F. M., Konokhova, Y., Rak, J., Chevalier, S., Taivassalo, T., Hepple, R. T., and Jagoe, R. T. (2015) Anthracycline-containing chemotherapy causes long-term impairment of mitochondrial respiration and increased reactive oxygen species release in skeletal muscle. *Sci. Rep.* **5,** 8717 CrossRef Medline
4. Bonifati, D. M., Ori, C., Rossi, C. R., Caira, S., Fanin, M., and Angelini, C. (2000) Neuromuscular damage after hyperthermic isolated limb perfusion in patients with melanoma or sarcoma treated with chemotherapeutic agents. *Cancer Chemother. Pharmacol.* **46,** 517–522 CrossRef Medline
5. Tozer, R. G., Tai, P., Falconer, W., Ducruet, T., Karabadjian, A., Bounous, G., Molson, J. H., and Dröge, W. (2008) Cysteine-rich protein reverses weight loss in lung cancer patients receiving chemotherapy or radiotherapy. *Antioxid. Redox Signal.* **10,** 395–402 CrossRef Medline
6. Stone, P., Hardy, J., Broadley, K., Tookman, A. J., Kurowska, A., and A'Hern, R. (1999) Fatigue in advanced cancer: a prospective controlled cross-sectional study. *Br. J. Cancer* **79,** 1479–1486 CrossRef Medline
7. Jacobsen, P. B., Hann, D. M., Azzarello, L. M., Horton, J., Balducci, L., and Lyman, G. H. (1999) Fatigue in women receiving adjuvant chemotherapy for breast cancer: characteristics, course, and correlates. *J. Pain Symptom Manage.* **18,** 233–242 CrossRef Medline
8. Bredahl, E. C., Pfannenstiel, K. B., Quinn, C. J., Hayward, R., and Hydock, D. S. (2016) Effects of exercise on doxorubicin-induced skeletal muscle dysfunction. *Med. Sci. Sports Exerc.* **48,** 1468–1473 CrossRef Medline
9. Gilliam, L. A., Ferreira, L. F., Bruton, J. D., Moylan, J. S., Westerblad, H., St Clair, D. K., and Reid, M. B. (2009) Doxorubicin acts through tumor necrosis factor receptor subtype 1 to cause dysfunction of murine skeletal muscle. *J. Appl. Physiol.* **107,** 1935–1942 CrossRef Medline
10. Bredahl, E. C., and Hydock, D. S. (2017) Creatine supplementation and doxorubicin-induced skeletal muscle dysfunction: an *ex vivo* investigation. *Nutr. Cancer* **69,** 607–615 CrossRef Medline
11. van Norren, K., van Helvoort, A., Argilés, J. M., van Tuijl, S., Arts, K., Gorselink, M., Laviano, A., Kegler, D., Haagsman, H. P., and van der Beek, E. M. (2009) Direct effects of doxorubicin on skeletal muscle contribute to fatigue. *Br. J. Cancer.* **100,** 311–314 CrossRef Medline
12. Hydock, D. S., Lien, C.-Y., Jensen, B. T., Schneider, C. M., and Hayward, R. (2011) Characterization of the effect of in vivo doxorubicin treatment on skeletal muscle function in the rat. *Anticancer Res.* **31,** 2023–2028 Medline
13. Gilliam, L. A., Lark, D. S., Reese, L. R., Torres, M. J., Ryan, T. E., Lin, C.-T., Cathey, B. L., and Neufer, P. D. (2016) Targeted overexpression of mitochondrial catalase protects against cancer chemotherapy-induced skeletal muscle dysfunction. *Am. J. Physiol. Endocrinol. Metab.* **311,** E293–E301 CrossRef Medline
14. Gilliam, L. A. A., Fisher-Wellman, K. H., Lin, C.-T., Maples, J. M., Cathey, B. L., and Neufer, P.D. (2013) The anticancer agent doxorubicin disrupts mitochondrial energy metabolism and redox balance in skeletal muscle. *Free Radic. Biol. Med.* **65,** 988–996 CrossRef Medline
15. Rossi, A. E., Boncompagni, S., and Dirksen, R. T. (2009) Sarcoplasmic reticulum-mitochondrial symbiosis: bidirectional signaling in skeletal muscle. *Exerc. Sport Sci. Rev.* **37,** 29–35 CrossRef Medline
16. Koopman, W. J., Renders, M., Oosterhof, A., van Kuppevelt, T. H., van Engelen, B. G., and Willems, P. H. (2003) Upregulation of Ca^{2+} removal in human skeletal muscle: a possible role for Ca^{2+}-dependent priming of mitochondrial ATP synthesis. *Am. J. Physiol. Cell Physiol.* **285,** C1263–C1269 CrossRef Medline
17. Shkryl, V. M., and Shirokova, N. (2006) Transfer and tunneling of Ca^{2+} from sarcoplasmic reticulum to mitochondria in skeletal muscle. *J. Biol. Chem.* **281,** 1547–1554 CrossRef Medline
18. Smuder, A. J., Kavazis, A. N., Min, K., and Powers, S. K. (2011) Exercise protects against doxorubicin-induced markers of autophagy signaling in skeletal muscle. *J. Appl. Physiol.* **111,** 1190–1198 CrossRef Medline
19. Sin, T. K., Tam, B. T., Yu, A. P., Yip, S. P., Yung, B. Y., Chan, L. W., Wong, C. S., Rudd, J. A., and Siu, P. M. (2016) Acute treatment of resveratrol alleviates doxorubicin-induced myotoxicity in aged skeletal muscle through SIRT1-dependent mechanisms. *J. Gerontol. A. Biol. Sci. Med. Sci.* **71,** 730–739 CrossRef Medline
20. Larsen, S., Nielsen, J., Hansen, C. N., Nielsen, L. B., Wibrand, F., Stride, N., Schroder, H. D., Boushel, R., Helge, J. W., Dela, F., and Hey-Mogensen, M. (2012) Biomarkers of mitochondrial content in skeletal muscle of healthy young human subjects. *J. Physiol.* **590,** 3349–3360 CrossRef Medline
21. Tarpey, M. D., Amorese, A. J., Balestrieri, N. P., Ryan, T. E., Schmidt, C. A., McClung, J. M., and Spangenburg, E. E. (2018) Characterization and utilization of the flexor digitorum brevis for assessing skeletal muscle function. *Skelet. Muscle* **8,** 14 CrossRef Medline
22. Murphy, R. M., Larkins, N. T., Mollica, J. P., Beard, N. A., and Lamb, G. D. (2009) Calsequestrin content and SERCA determine normal and maximal Ca^{2+} storage levels in sarcoplasmic reticulum of fast- and slow-twitch fibres of rat. *J. Physiol.* **587,** 443–460 CrossRef Medline
23. Loirat, M. J., Lucas-Heron, B., Ollivier, B., and Leoty, C. (1988) Calcium binding protein changes of sarcoplasmic reticulum from rat denervated skeletal muscle. *Biosci. Rep.* **8,** 369–378 CrossRef Medline
24. Hanna, A. D., Lam, A., Tham, S., Dulhunty, A. F., and Beard, N. A. (2014) Adverse effects of doxorubicin and its metabolic product on cardiac RyR2 and SERCA2A. *Mol. Pharmacol.* **86,** 438–449 CrossRef Medline
25. Asayama, J., Yamahara, Y., Tatsumi, T., Miyazaki, H., Inoue, M., Omori, I., Inoue, D., and Nakagawa, M. (1992) Acute effects of doxorubicin on skinned cardiac muscle fibres of guinea pigs. *Cardiovasc. Res.* **26,** 371–375 CrossRef Medline
26. Ondrias, K., Borgatta, L., Kim, D. H., and Ehrlich, B. E. (1990) Biphasic effects of doxorubicin on the calcium release channel from sarcoplasmic reticulum of cardiac muscle. *Circ. Res.* **67,** 1167–1174 CrossRef Medline
27. Saks, V. A., Khuchua, Z. A., Vasilyeva, E. V., Belikova, O., and Kuznetsov, A. V. (1994) Metabolic compartmentation and substrate channelling in muscle cells: role of coupled creatine kinases in *in vivo* regulation of cellular respiration: a synthesis. *Mol. Cell. Biochem.* **133-134,** 155–192 CrossRef Medline
28. Janssen, E., Terzic, A., Wieringa, B., and Dzeja, P. P. (2003) Impaired intracellular energetic communication in muscles from creatine kinase and adenylate kinase (M-CK/AK1) double knock-out mice. *J. Biol. Chem.* **278,** 30441–30449 CrossRef Medline

29. Yi, J., Ma, C., Li, Y., Weisleder, N., Ríos, E., Ma, J., and Zhou, J. (2011) Mitochondrial calcium uptake regulates rapid calcium transients in skeletal muscle during excitation–contraction (E–C) coupling. *J. Biol. Chem.* **286,** 32436–32443 CrossRef Medline
30. McLaughlin, K. L., McClung, J. M., and Fisher-Wellman, K. H. (2018) Bioenergetic consequences of compromised mitochondrial DNA repair in the mouse heart. *Biochem. Biophys. Res. Commun.* **504,** 742–748 CrossRef Medline
31. Cunha-Oliveira, T., Ferreira, L. L., Coelho, A. R., Deus, C. M., and Oliveira, P. J. (2018) Doxorubicin triggers bioenergetic failure and p53 activation in mouse stem cell-derived cardiomyocytes. *Toxicol. Appl. Pharmacol.* **348,** 1–13 CrossRef Medline
32. Pawelczyk, T., and Olson, M. S. (1992) Regulation of pyruvate dehydrogenase kinase activity from pig kidney cortex. *Biochem. J.* **288,** 369–373 CrossRef Medline
33. Murakami, T., Matsuo, M., Shimizu, A., and Shimomura, Y. (2005) Dissociation of branched-chain α-keto acid dehydrogenase kinase (BDK) from branched-chain α-keto acid dehydrogenase complex (BCKDC) by BDK inhibitors. *J. Nutr. Sci. Vitaminol.* (*Tokyo*) **51,** 48–50 CrossRef Medline
34. Gammella, E., Maccarinelli, F., Buratti, P., Recalcati, S., and Cairo, G. (2014) The role of iron in anthracycline cardiotoxicity. *Front. Pharmacol.* **5,** 25 Medline
35. Cappetta, D., De Angelis, A., Sapio, L., Prezioso, L., Illiano, M., Quaini, F., Rossi, F., Berrino, L., Naviglio, S., and Urbanek, K. (2017) Oxidative stress and cellular response to doxorubicin: a common factor in the complex milieu of anthracycline cardiotoxicity. *Oxid. Med. Cell. Longev.* **2017,** 1521020 Medline
36. Ichikawa, Y., Naik, J., Ardehali, H., Ghanefar, M., Bayeva, M., Wu, R., Khechaduri, A., Naga Prasad, S. V., Mutharasan, R.K., Naik, T. J., and Ardehali, H. (2014) Cardiotoxicity of doxorubicin is mediated through mitochondrial iron accumulation. *J. Clin. Invest.* **124,** 617–630 CrossRef Medline
37. Simunek, T., Stérba, M., Popelová, O., Adamcová, M., Hrdina, R., and Gersl, V. (2009) Anthracycline-induced cardiotoxicity: overview of studies examining the roles of oxidative stress and free cellular iron. *Pharmacol. Rep.* **61,** 154–171 Medline
38. Xu, X., Persson, H. L., and Richardson, D. R. (2005) Molecular pharmacology of the interaction of anthracyclines with iron. *Mol. Pharmacol.* **68,** 261–271 CrossRef Medline
39. Gilliam, L. A., Moylan, J. S., Patterson, E. W., Smith, J. D., Wilson, A. S., Rabbani, Z., and Reid, M. B. (2012) Doxorubicin acts via mitochondrial ROS to stimulate catabolism in C2C12 myotubes. *Am. J. Physiol. Cell Physiol.* **302,** C195–C202 CrossRef Medline
40. Keizer, H. G., Pinedo, H. M., Schuurhuis, G. J., and Joenje, H. (1990) Doxorubicin (adriamycin): a critical review of free radical-dependent mechanisms of cytotoxicity. *Pharmacol. Ther.* **47,** 219–231 CrossRef Medline
41. Xu, W., Barrientos, T., and Andrews, N. C. (2013) Iron and copper in mitochondrial diseases. *Cell Metab.* **17,** 319–328 CrossRef Medline
42. Committee for the Update of the Guide for the Care and Use of Laboratory Animals (2011) *Guide for the Care and Use of Laboratory Animals*, 8th Ed., National Academies Press, Washington, D. C.
43. Freireich, E. J., Gehan, E. A., Rall, D. P., Schmidt, L. H., and Skipper, H. E. (1966) Quantitative comparison of toxicity of anticancer agents in mouse, rat, hamster, dog, monkey, and man. *Cancer Chemother. Rep.* **50,** 219–244 Medline
44. Schmidt, C. A., Ryan, T. E., Lin, C.-T., Inigo, M. M. R., Green, T. D., Brault, J. J., Spangenburg, E. E., and McClung, J. M. (2017) Diminished force production and mitochondrial respiratory deficits are strain-dependent myopathies of subacute limb ischemia. *J. Vasc. Surg.* **65,** 1504–1514.e11 CrossRef Medline
45. Brooks, S. V, and Faulkner, J. A. (1988) Contractile properties of skeletal muscles from young, adult and aged mice. *J. Physiol.* **404,** 71–82 CrossRef Medline
46. Tupling, R., Green, H., Senisterra, G., Lepock, J., and McKee, N. (2001) Effects of ischemia on sarcoplasmic reticulum Ca^{2+} uptake and Ca^{2+} release in rat skeletal muscle. *Am. J. Physiol. Metab.* **281,** E224–E232 CrossRef Medline
47. O'Brien, P. J. (1990) Calcium sequestration by isolated sarcoplasmic reticulum: real-time monitoring using ratiometric dual-emission spectrofluorometry and the fluorescent calcium-binding dye indo-1. *Mol. Cell. Biochem.* **94,** 113–119 CrossRef Medline
48. Golding, E. M., Teague, W. E., Jr., and Dobson, G. P. (1995) Adjustment of K′ to varying pH and pMg for the creatine kinase, adenylate kinase and ATP hydrolysis equilibria permitting quantitative bioenergetic assessment. *J. Exp. Biol.* **198,** 1775–1782 Medline
49. Teague, W. E., Jr., Golding, E. M., and Dobson, G. P. (1996) Adjustment of K′ for the creatine kinase, adenylate kinase and ATP hydrolysis equilibria to varying temperature and ionic strength. *J. Exp. Biol.* **199,** 509–512 Medline
50. Fisher-Wellman, K. H., Davidson, M. T., Narowski, T. M., Lin, C.-T., Koves, T. R., and Muoio, D. M. (2018) Mitochondrial diagnostics: a multiplexed assay platform for comprehensive assessment of mitochondrial energy fluxes. *Cell Rep.* **24,** 3593–3606.e10 CrossRef Medline
51. Scaduto, R. C., Jr., and Grotyohann, L. W. (1999) Measurement of mitochondrial membrane potential using fluorescent rhodamine derivatives. *Biophys. J.* **76,** 469–477 CrossRef Medline
52. Tarpey, M. D., Valencia, A. P., Jackson, K. C., Amorese, A. J., Balestrieri, N. P., Renegar, R. H., Pratt, S. J. P., Ryan, T. E., McClung, J. M., Lovering, R. M., and Spangenburg, E. E. (2019) Induced *in vivo* knockdown of the Brca1 gene in skeletal muscle results in skeletal muscle weakness. *J. Physiol.* **597,** 869–887 CrossRef Medline